PCCP

Accepted Manuscript

ROYAL SOCIETY OF CHEMISTRY

www.rsc.org/pccp

Mika Niskanen and Terttu I. Hukka

Modeling of Photoactive Conjugated Donor–Acceptor Copolymers: The Effect of the Exact HF Exchange in DFT Functionals on Geometries and Gap Energies of Oligomer and Periodic Models

GRAPHICAL ABSTRACT

Commonly used density functionals including an optimally tuned OT-ωB97X functional are benchmarked on oligomer and periodic models of donor–acceptor copolymers.

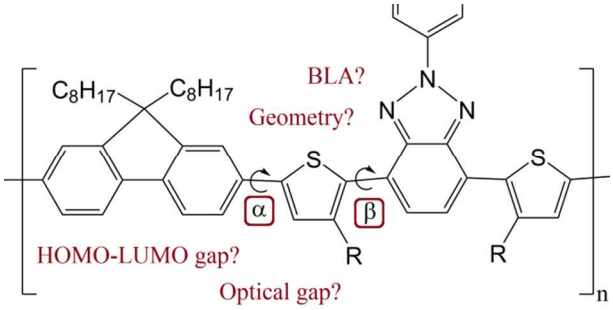

Modeling of Photoactive Conjugated Donor–Acceptor Copolymers: The Effect of the Exact HF Exchange in DFT Functionals on Geometries and Gap Energies of Oligomer and Periodic Models

M. Niskanen,[a] T. I. Hukka[a]

Correspondence to: T. I. Hukka (Email: *terttu.hukka@tut.fi*)

ABSTRACT

Conjugated copolymers with an alternating donor–acceptor (D–A) architecture are exploited as low-bandgap and high-hole-mobility materials in organic electronics. However, several of the presently available modeling methods predict different geometries and electronic properties for the same copolymer. In this work, the effect of the amount of exact Hartree-Fock (HF) exchange in density functionals on the planarity of the geometry and the electronic properties of the single oligomer chains of one benzodithiophene- and benzotriazole-based donor–acceptor copolymer and two fluorene-, thiophene-, and benzotriazole-based donor–acceptor copolymers is assessed. The functionals are B3LYP, PBE, PBE0, HSE06, LC-ωPBE, ωB97XD, M06, M06L, M062X, M06HF, and the optimally tuned OT-ωB97X. Benchmarking the methods is useful for understanding the results of a particular functional and allows, to a certain degree, comparison between results obtained with different functionals. Additionally, the applicability of the one-dimensional periodic boundary condition (PBC) for modeling the D–A copolymers with long constitutional repeating units (CRUs) is evaluated.

Keywords: Donor–acceptor copolymers, conjugated polymers, density functional theory, periodic boundary conditions, optimally tuned functional

Introduction

Relatively low fabrication cost and easy manufacturing make conjugated polymers promising materials for light-emitting diodes,[1,2] field-effect transistors,[3] organic solar cells,[4,5] and chemical sensors.[6,7,8] Conjugated polymers with a donor–acceptor (D–A) architecture have drawn special attention, because alternation of the electron deficient and electron rich moieties in the polymer backbone has been discovered to lower the band gap.[9,10] This is important for example in photovoltaic devices, in which the band gap of the conjugated polymer determines the maximum photo-excitation wavelength. However, at the same time a lower band gap means a lower voltage in the cell. Conjugated polymers with low band gaps are useful for example in organic solar cells that absorb light mainly in the infrared region and are transparent to the human eye[11] or in the so called tandem polymer photovoltaic cells. In a tandem cell two cells are combined: the first cell collects light at lower wavelengths while the second cell, that has a lower band gap, collects light at the higher wavelengths. Recently a certified record efficiency of 10.6 % has been achieved with a tandem polymer solar cell.5

The need to understand the properties of conjugated polymers at the molecular level has stimulated also computational research on top of the plentiful experimental studies. Most commonly, the polymers used in experimental devices are examined computationally to further the understanding of the origins of their electronic properties. In addition, new suitable materials are screened. Usually, the polymers are studied by

modeling isolated oligomers of increasing length using density functional theory (DFT) and fitting the calculated structural or electronic properties either as a function of the inverse of *n* (1/*n*), where *n* is the number of the constitutional repeating units (CRUs), or as a function of the inverse of the number of the double bonds (*N*) along the shortest path of the polymer backbone, thus yielding an extrapolation for the polymer properties.[12,13,14,15,16,17,18,19] The energy gap between the highest occupied molecular orbital (HOMO) and the lowest unoccupied molecular orbital (LUMO), *i.e.* the HOMO–LUMO gap as called hereafter, is one of the properties of interest and can be evaluated directly from the Kohn–Sham eigenvalues. Additionally, excitation energies can be estimated with the time-dependent density functional theory (TD-DFT).

A less applied approach, but a good alternative for the fitting procedure, is to employ periodic boundary conditions (PBCs) in the calculations and to build an isolated one-dimensional (1D) polymer model.[20,21,22,23,24,25] This way the desired properties of the polymer are directly obtained from the calculations, but some freedom of the geometry is possibly lost and comparison with the fully-relaxed oligomers is not reasonable if the geometries of the oligomer and polymer models are too different. Moreover, the possibilities to study such properties as ionization potential and electron affinity using charged species or the excited states using the TD-DFT formalism are lost, because these properties have not been implemented in many computational codes that have PBCs.

Both in the fitting to the polymer limit and in using the PBC model it is important to remember that information is obtained only on long, conjugated polymers. Such approximation is valid only for crystalline or very rigid polymers, whereas in other cases defects, i.e. for example structural deviations from the PBC geometry, are likely to weaken or break the conjugation.[26] Moreover, it is good to keep in mind that the information is obtained only from the middle part of an infinitely long polymer, whereas the terminating ends and their effects can be assessed only from the oligomer models.

In some of the previous studies, the models of the conjugated polymers extend beyond single polymer backbones, as in the cases of interfaces[27,28] and blends.[29] Because polymers are often either in a fully amorphous morphology or contain only small crystalline regions, the models describing the structures need to be large in which cases the applicable level of theory is restricted to molecular mechanics or semiempirical methods. On the other hand, smaller crystalline or molecular models are built when local interactions on interfaces are studied with more accurate methods.[30,31,32]

The B3LYP hybrid density functional is still a popular choice for studying oligomer or 1D polymer models of conjugated polymers. However, novel functionals, such as the screened hybrid HSE06, Minnesota, and various long-range-corrected functionals are attracting and drawing more attention.[21~~21~~,32,33] Especially, the long-range-corrected functionals have been introduced as promising alternatives for predicting *e.g.* ionization energies, excitations energies, and orbital energies accurately for conjugated oligomers.[33~~32~~] The long-range corrected functionals contain a large amount of HF exchange for long electron-electron distances and may contain a large amount of DFT exchange for short electron-electron distances.[34] Splitting between the long-range and short-range terms can be done for example by standard error function (erf) splitting operator (equation 1), where r_{12} is the distance between two electrons $|\mathbf{r_1}\text{-}\mathbf{r_2}|$. Moreover, by tuning the range-separation parameter ω it is possible to predict the fundamental gaps and excitation energies with a good accuracy.[35,36]

$$\frac{1}{r_{12}} = \frac{erf(\omega r_{12})}{r_{12}} + \frac{erfc(\omega r_{12})}{r_{12}} \qquad (1)$$

In the present work, we have evaluated the relative performances of the Hartree–Fock (HF) wave function method, the PM6 semiempirical method, and density functional theory using 11 different functionals, *i.e.* B3LYP, PBE, PBE0, HSE06, LC-ωPBE, ωB97XD, OT-ωB97X, M06, M06L, M062X, and M06HF when modeling three D–A copolymers[37,38] P1, P2, and P3 (see Figure 1). A specific attention has been paid to the optimally tuned OT-ωB97X functional because of the novelty of OT functionals and their promising accuracy for predicting fundamental gaps and excitation energies. The chemical name of P1 is poly{2-(4-(decyloxy)-3,5-difluorophenyl)-2H-benzo[d][1,2,3]triazole-4,7-diyl-4,8-bis((2-ethylhexyl)oxy)benzo[1,2-b:4,5-b']dithiophene-2,6-diyl}, the P2 is poly{2-(4-(decyloxy)-3,5-difluorophenyl)-2H-benzo[d][1,2,3]triazole-4,7-diyl-thiophen-2,5-yl-9,9-dioctyl-9H-fluorene-2,7-diyl-thiophen-2,5-diyl} and the P3 is poly{2-(4-(decyloxy)-3,5-difluorophenyl)-2H-benzo[d][1,2,3]triazole-4,7-diyl-3-hexylthiophen-2,5-yl-9,9-dioctyl-9H-fluorene-2,7-diyl-3-hexylthiophen-5,2-diyl}.[39] P1 has a linear planar backbone, P2 a curved planar backbone, and P3 a curved backbone that is not planar. The properties evaluated are geometries, *i.e.* the dihedral angles between the donor and acceptor units in the backbone of the copolymer, bond length alternation (BLA), the HOMO–LUMO gaps calculated from the orbital eigenvalues, the first excitation energies predicted by the TD-DFT formalism, and the electron density distributions of the frontier molecular orbitals (FMOs). Furthermore, we have assessed the applicability of the one-dimensional PBCs for modeling of polymer chains using the methods mentioned above.

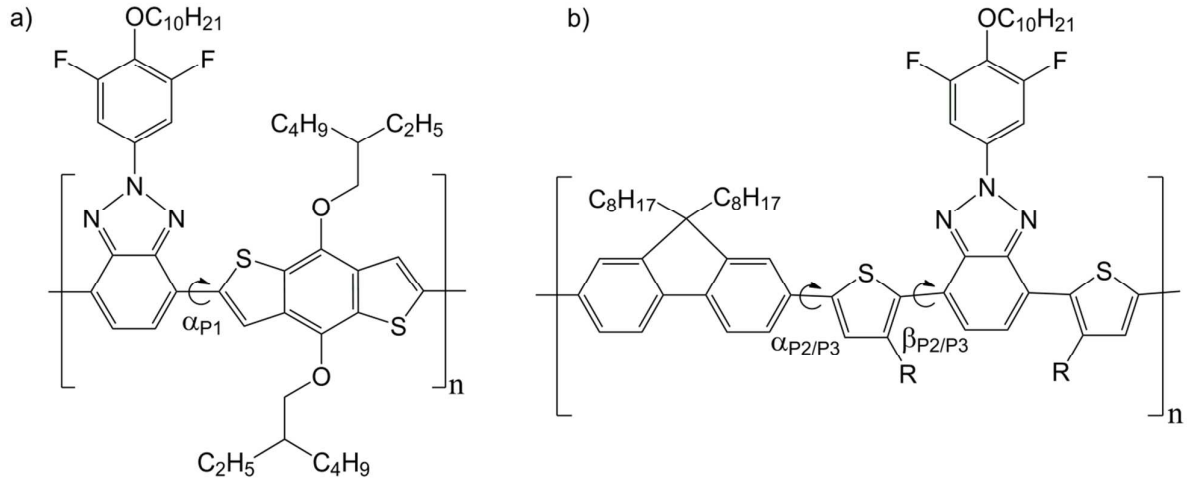

Figure 1. Constitutional repeating units of a) P1, b) P2 (R = H), and P3 (R = C_6H_{13}).

Methods

Computational Software and Methodology

All calculations were carried out using the Gaussian 09 program package.[40] We employed the Hartree–Fock wavefunction and the PM6 semiempirical method[41] as well as DFT with 11 different functionals. The DFT functionals include: two pure density functionals, PBE[42,43] and M06L;[44] the commonly used global hybrid functionals, B3LYP[45,46,47,48] and PBE0;[42,43,49] the similarly behaving M06[50] functional; the long-range-corrected functionals, LC-ωPBE,[51,52] M06-HF,[53,54] and ωB97XD,[55] of which ωB97XD includes the empirical dispersion correction;[56] the optimally tuned OT-ωB97X[34] functional, where the range-separation parameter ω has been tuned to produce the fundamental gap accurately by enforcing Koopmans' theorem.[35,57,58] the M06-2X functional,[50] that has twice the amount of the exact HF exchange compared to M06; and the screened-hybrid HSE06 functional,[59,60,61,62] which has been developed for solid state calculations and often yields results similar to those given by PBE0, but faster.

The 6-31G* basis set was used in the HF and DFT calculations. Geometries, orbitals, orbital energies, and the HOMO–LUMO gaps of the optimized structures were analyzed using Chemcraft.[63] Frequencies were calculated for the monomers (n = 1) to ensure that the geometries were at the energy minima. In addition, the TD-HF and TD-DFT formalisms were used to evaluate the first excitation energies of the oligomer models, which are discussed below. Additional OT-ωB97X single point TD-DFT calculations were performed with the 6-31+G(d,p) basis set and the integral equation formalism variant of the polarizable continuum model[64] was used to add chloroform as the solvent. The same range-separation parameter (ω) values were used as for the 6-31G(d) calculations.

Models

The constitutional repeating units of the alternating D–A copolymers studied in this work compose of an electron rich donor and an electron deficient acceptor. The models were either short oligomers or polymer chains that were created using periodic boundary conditions (defined by the translation vector Tv in the geometry input). The oligomer models of P1 have (n = 1–8) while those of P2 and P3 have (n = 1–4). The default number of the k-points was used in the periodic calculations. The number of the k-points depends on the length of Tv, which is ca. 13 Å, 38 Å, and 38 Å, and translated into 27, 9, and 9 k-points in the periodic models of P1, P2, and P3 (Figure 2), respectively. The solubility enhancing long alkoxy side chains, $–OC_{10}H_2$ and $–OCH_2CH(C_2H_5)C_4H_9$, were replaced by $–OCH_3$ and the long alkyl side chains, $–C_6H_{13}$ and $–C_8H_{17}$, by $–CH_3$ to reduce the computational time.

The DFT/B3LYP/6-31G* optimized geometries of the P1 and P2 models were adopted from our previous study[38,65,66] and used as the initial structures for the geometry optimizations applying the methods presented above. Potential energy surface scans with the B3LYP functional were done to identify the energy difference between the conformational isomers. Only the lowest energy conformational isomer (within the chosen PBC) for each polymer was considered as the focus was in comparing the methods. The initial oligomer model of P1 had a linear and slightly spiral backbone with alternating (10–15) and (0–3) degree dihedral angles between the donor and the acceptor units, while the periodic model had alternating dihedral angles of 4 and -4 degrees creating practically a planar polymer. The initial oligomer model of P2 had a planar zigzag backbone with dihedral angles of (2–10) degrees between the thiophene and benzotriazole units and of (22–25) degrees between the thiophene and fluorene units. The periodic model of P2 was constructed of two CRUs to create a relaxed and repeatable structure. In the optimized periodic model the dihedral angles were ca. 9 degrees between thiophene and benzotriazole and (19–25) degrees between thiophene and fluorene making a polymer with a planar zigzag backbone. We also built the oligomer and periodic models with zigzag backbones for P3. The periodic model of P3 consists also of two

CRUs. The initial B3LYP/6-31G* geometry had dihedral angles of ca. 48 degrees between the 3-methylthiophene and benzotriazole units due to the steric repulsion caused by the substituent in thiophene. The oligomer and polymer models of P3 are otherwise similar to the zigzag models of P2, but the backbone is wavy, because the substituents prevent the planarity.

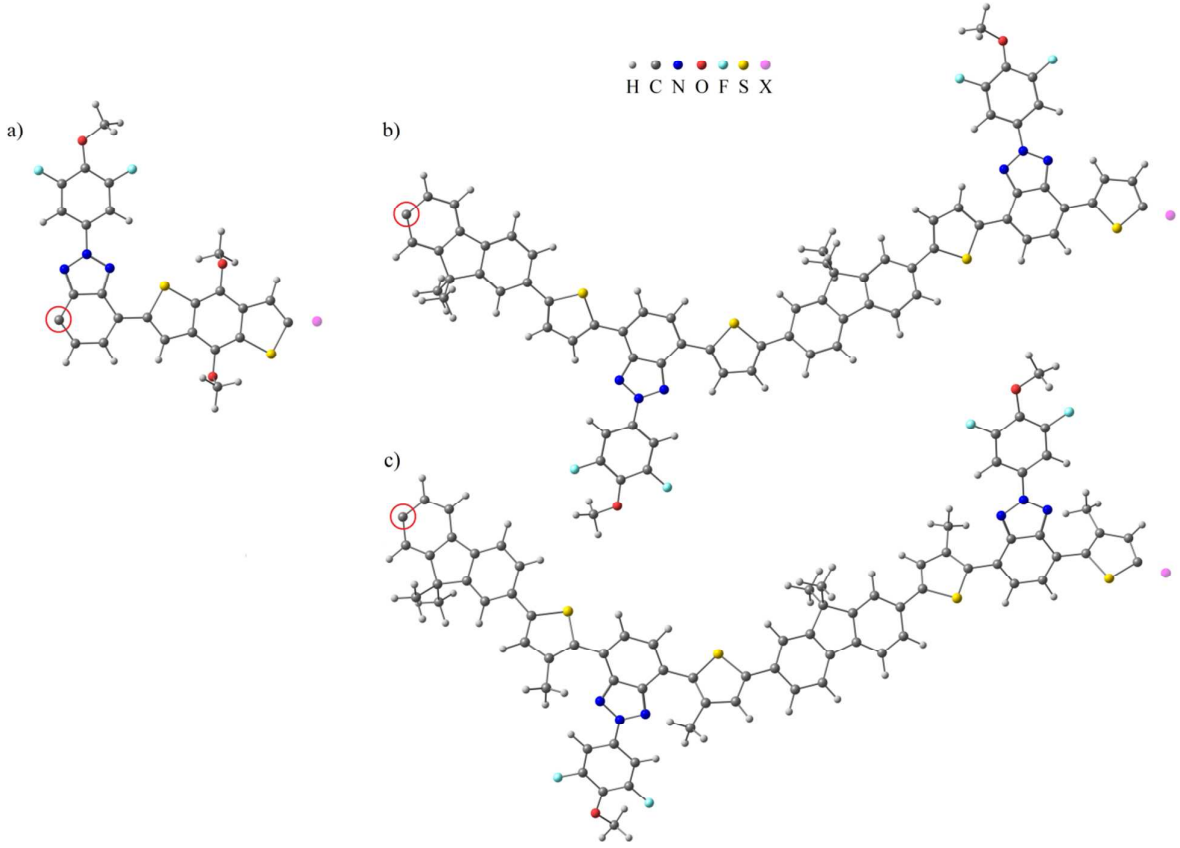

Figure 2. Periodic models of a) P1, b) P2, and c) P3 optimized at the B3LYP/6-31G* level of theory. Each structure is copied from the circled carbon atom to the position of the pink dummy-atom by the translation vector Tv.

Bond length alternation

Bond length alternation (BLA) provides information about such properties as the conjugation length, molecular dipole moment, polarizability, and hyperpolarizabilities of a conjugated system.[67] It is also used to inspect the structural differences between the electronic ground and excited states.[68] The BLA can be calculated for a specific path in a molecule by taking an average value of the single bond lengths in the path and subtracting from it an average value of the double bond lengths along the same path. If the subtraction is done in this order, a positive BLA value is a measure of the conjugational character and in the case of cyclically conjugated molecular entities a measure of aromatic character, *i.e.* the larger the BLA value, the stronger the conjugation. However, a value close to zero means that the structure is a resonance hybrid, *i.e.* there are shared delocalized π-electrons, as in a benzene ring. For an excited state the BLA value is commonly negative, because the electron density transfers from the double bonds to the single bonds, which lengthens the double bonds and shortens the single bonds. We calculated the BLA values for the ground states of the periodic models of P1–P3.

Extrapolation methods

There are many ways to fit the oligomer HOMO–LUMO gap results and to extrapolate the gap value at the polymer limit.[19~~19~~] In this study Kuhn fit,[69] linear fit, and 2nd to 4th order polynomial fits were tested. Even though Kuhn fit usually gives good band gap estimates for conjugated polymers, when the CRU is short,[19~~19~~] it did not work well in the case of our polymers. One reason for this can be that the polymers P1–P3 have long CRUs, which leads to fewer data points for the extrapolation and all the points are located at low $1/n$ values (≤ 0.16) where the changes in the HOMO–LUMO gap are small. Another reason can be that the polymers P1–P3 are copolymers in which the building components of one CRU have HOMOs (and LUMOs) at different energies. Moreover, the linear fit, on the other hand, yields too low HOMO–LUMO gaps. For these reasons we employed polynomial fits for the extrapolation. With each computational method and with each set of the oligomers P1, P2, and P3, we chose the lowest order polynomial fit, that (1) gave a larger HOMO–LUMO gap than the linear fit for the two longest oligomers, (2) was descending all the way to the polymer limit, and (3) was yielding a smaller derivative of the fitting curve as it approached the polymer limit; the derivative was not forced to zero at the polymer limit although it was considered.

Tuning of the range-separation parameter

The range-separation parameter (ω) of a given range-separated density functional can be tuned for each chemical system of interest to produce the fundamental gaps more accurately. This is achieved by minimizing J^2 of equation (2).[35~~35~~,57]

$$J^2(\omega) = \left(\varepsilon^{\omega}_{HOMO(N)} + IE^{\omega}(N)\right)^2 + \left(\varepsilon^{\omega}_{HOMO(N+1)} + IE^{\omega}(N+1)\right)^2 \qquad (2)$$

This effectively enforces Koopmans' theorem by minimizing the difference between the ionization energy (IE) and $-\varepsilon_{HOMO}$ of the molecule and its N+1 anion. The range separation parameter of the ωB97X functional, originally 0.30 $bohr^{-1}$, was tuned to obtain an optimally tuned OT-ωB97X functional. The parameter was optimized for the P1–P3 monomers giving the values of 0.16, 0.14, and 0.14 $bohr^{-1}$, respectively, and for the longest oligomer models (n=8 for P1, n=4 for P2, and P3), giving values of 0.10, 0.12, and 0.14 $bohr^{-1}$, respectively. After this the values obtained for the longest oligomer models were used in periodic calculations. The optimal tuning indicates that the original value was too high for the studied systems and that the OT-ωB97X functional allows more delocalization than the other long-range corrected functionals considered in this study.

Results and Discussion

Amount of the exact HF exchange in the density functionals

Because we refer to the amount of the exact HF exchange in the functional when the results are discussed, we introduce the functionals shortly. For the pure density functionals the amount of the exact HF exchange is zero and for some hybrid functionals the amount of HF exchange is given as a single value. However, the HSE06 functional can be considered to work as the PBE0 functional at short interatomic distances and as the PBE functional at long interatomic distances, whereas the long range ω functionals contain a large amount of the HF exchange in general but less at short interatomic distances. We have calculated the effective HF exchange[70] by plotting the HOMO–LUMO gaps of the periodic P1–P3 models as a function of the HF exchange for the DFT methods, for which it is given as a simple predefined multiplier, and used linear regression to obtain an approximation of the effective HF exchange in the cases of the HSE06 and ω

functionals (see ESI). For simplicity, the changes in the HOMO–LUMO gap obtained with different functionals are presumed to originate solely from the addition of the exact HF exchange to the functionals even though the DFT correlation and exchange parts of the functionals are also different. The amounts of the HF exchange in different functionals are presented in Table 1. In the text M062X, OT-ωB97X, ωB97XD, LC-ωPBE, and M06HF are sometimes collectively referred to as the high HF exchange methods.

Table 1. Amounts (%) of the HF exchange present in the density functionals included in this study.

PBE	M06L	HSE06	B3LYP	PBE0	M06	M062X	OT-ωB97X	ωB97XD	LC-ωPBE	M06HF
0	0	12–13[a]	21	25	27	54	56-65[a]	79–80[a]	97–98[a]	100

[a] An effective HF exchange, see the text for the details.

Effect of the method on the geometries of the D–A polymers

The investigated polymers have no strong planarity enforcing intramolecular interactions. As a result the modeling method affects especially the dihedral angle of the D–A polymer backbone. To demonstrate this we have compared the dihedral angles α and β (see Figure 1) predicted by each method for the optimized structures of the periodic models and the oligomer models, which consist of 4 CRUs (Table 2). In the oligomer models dihedral angles of the two innermost CRUs are examined.

Table 2. Dihedral angles α and β (in degrees) in the two innermost backbone CRUs of the oligomer models with n = 4 and in the periodic (PBC) models P1–P3.

Method	α_{P1}		α_{P2}		β_{P2}		α_{P3}		β_{P3}	
	oligomer[a]	PBC	oligomer	PBC	oligomer	PBC	oligomer	PBC	oligomer	PBC
PBE	2 / 4	0	20	17	3	5	21	22	45	42
M06L	2 / 5	3	11	12	2	2	16	16	42	40
HSE06	1 / 12	2	23	22	5	8	25	25	46	44
B3LYP	0 / 15	4	24	22	5	8	25	25	48	46
PBE0	1 / 16	4	25	23	6	9	26	26	47	45
M06	5 / 14	3	23	22	7	8	25	25	45	43
M06-2X	9 / 21	12	28	27	10	11	28	28	46	45
OT-ωB97X[b]	9 / 29	21	31	31	16	14	31	32	49	49
ωB97XD	12 / 27	17	32	31	14	13	32	32	50	49
LC-ωPBE	8 / 31	22	33	32	18	15	33	33	52	51
M06-HF	15 / 30	22	37	37	20	17	37	37	49	48
HF	18 / 43	32	37	37	24	19	38	38	57	56
PM6	2 / 28	-	48	-	29	-	48	-	54	-

[a] The P1 oligomer model has alternating α_{P1} dihedral angles, see the text for details. [b] The angle was measured for the OT-ωB97X n=8 model in the absence of an n=4 model.

As expected, there is a clear correlation between the amount of the exact HF exchange in the method and the value of the backbone dihedral angle in both the oligomer and periodic models. Namely, when the amount of the HF exchange increases the dihedral angle increases. Even in the most planar polymer, P1, the backbone dihedral angle clearly deviates from planarity when the method has a large amount of HF

exchange or when the mere HF method itself is used. The same trend is visible in the cases of the P2 and P3 models, as well. The OT-ωB97X functional yields similar dihedral angles to the other high HF exchange methods.

Moreover, the dihedral angles of the oligomer models and the PBC models can be compared in order to see whether the PBC models perform well, *i.e.* resemble the fully relaxed oligomer model or, for example, whether they restrict the geometry. Indeed, some differences are seen between the P1 oligomer models and the periodic models. In the periodic model of P1 all dihedral angles in the backbone are of the same size. However, the oligomer models with n = 2–8 have two alternating dihedral angles. The smaller dihedral angle is related to the slightly attractive and stabilizing N - - H interaction between benzodithiophene and benzotriazole and the larger dihedral angle to the conformation in which the sterically less unfavorable, equilibrium structure is reached when N and S are on the same side, which does not necessarily mean that they are interacting with each other.[71] The periodic model with only one CRU does not have geometric freedom for two distinct dihedral angles (the second angle must be of the same size but opposite in direction). Additional geometric freedom can be given to the model by incorporating e.g. two CRUs into the period. Addition of the second CRU to the model stabilizes the structure by 6 kJ/mol/CRU (B3LYP) because the nitrogen and sulphur atoms are located always on the opposite sides of the model, leading to a sterically slightly more favorable conformation. However, the HOMO–LUMO gap increases only by 0.06 eV (B3LYP). All in all, these findings are in line with the changes found between different conformational isomers of conjugated polymers.[72] However, we used only the periodic P1 model consisting of one CRU as its size and the HOMO–LUMO gap results are suitable for comparing the methods.

The dihedral angles, α and β, of the oligomer models of P2 and P3 vary only slightly from those of the corresponding periodic models, see Table 2. The dihedral angle α between fluorene and thiophene is almost the same regardless of the model and the dihedral angle β between thiophene and benzotriazole is the same within (2–3) degrees in both models. The deviations are possibly caused by the shortness of the oligomer chain compared to the chain length in the corresponding periodic model. As a summary, the PBC models produce corresponding geometries with the oligomer models, but the models have to be built carefully. Additionally, we stress that when evaluating the following results, it is good to keep in mind that the information is obtained only from the middle part of an infinitely long polymer, whereas the terminating ends and their effects can be assessed only from the oligomer models.

The PM6 semiempirical method was included into the study in order to see whether it can predict geometries comparable to those predicted by the DFT or HF methods and whether it can be used for preoptimizing the oligomer models or for studying amorphous packing of polymers that have similar structures to P1–P3. PM6 yields results close to those given by the high HF exchange DFT methods in the case of P1. In the cases of P2 and P3 both dihedral angles α and β are comparable to those given by HF and often greater. It appears that PM6 produces geometries that are not comparable to those predicted by other methods used in this study. As such, the PM6 method offers only a limited usage for polymers that have weak backbone interactions like P1–P3 here, but is perhaps more suitable for polymers, in which the donor–acceptor units have stronger intramolecular interactions leading to more rigid geometries.

We have calculated the BLA values for the ground states of the periodic models of P1–P3, see Table 3. The bond paths and the bond lengths are given in the ESI.

Table 3. BLA (Å) for the periodic models of P1–P3.

Method	P1	P2	P3
PBE	0.020	0.027	0.033
M06L	0.022	0.028	0.034
HSE06	0.031	0.036	0.043
B3LYP	0.033	0.039	0.046
PBE0	0.034	0.039	0.044
M06	0.035	0.040	0.045
M06-2X	0.047	0.050	0.054
OT-ωB97X	0.040	0.045	0.052
ωB97XD	0.050	0.052	0.057
LC-ωPBE	0.059	0.059	0.063
M06-HF	0.065	0.065	0.068
HF	0.074	0.073	0.079
PM6[a]	0.049	0.060	0.061

[a] Cannot be used with PBCs. For symmetry reasons, measured from the middle CRU of an oligomer model with n = 7 for P1 and n = 3 for P2 and P3.

The pure DFT functionals, PBE and M06L, predict quite small BLA values, meaning that the π-electrons are more delocalized along the bonds. However, the methods with larger amounts of the exact HF exchange predict larger BLA values. In other words, the differences between the lengths of the double and single bonds are larger when the method has more of the exact HF exchange. This is in agreement with the smaller amounts of the long-range electron delocalization built into these methods. The OT-ωB97X functional yields the smallest BLA values of the high HF exchange methods. This means that optimally tuning the range-parameter increases the delocalization for P1–P3 although there is still less delocalization than in the hybrid functionals. Moreover, the delocalization of the π-electrons along the bond paths of the polymers decreases in the order of P1 > P2 > P3.

All things considered, the computed geometry (*e.g.* the dihedral angle and the BLA) depends on the method chosen in this work, be it HF, DFT, or semiempirical. Therefore, the electronic properties for the polymers P1–P3 are also expected to depend on the method, i.e. the distribution of the electron density in the model.

Effect of the method on the HOMO–LUMO gaps of the D–A copolymers P1–P3

The methods were further evaluated by inspecting the predicted HOMO–LUMO gaps or the gaps between the highest occupied crystal orbital (HOCO) and the lowest unoccupied crystal orbital (LUCO), i.e. the HOCO–LUCO gaps, in the cases of the periodic models. The gaps of the longest oligomers, the gaps extrapolated from the oligomer data, and the gaps of the periodic (PBC) models of P1–P3 are listed in Table 4. The HOMO–LUMO gaps as a function of the oligomer length are given in ESI.

Table 4. HOMO–LUMO gaps (eV) of the longest oligomers, the extrapolated HOMO–LUMO gaps (eV), and the HOCO–LUCO gaps (eV).

Method	P1			P2			P3		
	n=8	extrapolated	PBC	n=4	extrapolated	PBC	n=4	extrapolated	PBC
PBE	1.04	0.97	1.00	1.28	1.18	1.22	1.50	1.42	1.46
M06L	1.18	1.10	1.13	1.38	1.27	1.33	1.63	1.53	1.59
HSE06	1.71	1.63	1.62	1.97	1.86	1.91	2.29	2.20	2.24
B3LYP	2.10	2.03	2.01	2.35	2.25	2.30	2.69	2.61	2.65
PBE0	2.39	2.31	2.29	2.67	2.56	2.61	3.01	2.93	2.96
M06	2.46	2.39	2.37	2.74	2.63	2.68	3.03	2.94	2.99
M06-2X	4.01	3.96	3.92	4.32	4.22	4.27	4.68	4.60	4.63
OT-ωB97X	4.15	-	4.11	4.71	-	4.66	5.36	-	5.33
ωB97XD	5.55	5.45	5.47	5.84	5.70	5.79	6.23	6.18	6.21
LC-ωPBE	6.55	6.49	6.49	6.91	6.79	6.84	7.34	7.28	7.30
M06-HF	6.77	6.71	6.69	7.17	7.06	7.11	7.53	7.48	7.49
HF	7.62	7.56	7.57	7.79	7.64	7.68	8.30	8.28	8.27
PM6	5.91	5.86	-	6.68	6.61	-	6.85	6.83	-

As expected, the HOMO–LUMO gap energy increases as the amount of the exact HF exchange in the method increases. The OT-ωB97X functional yields smaller HOMO–LUMO gap values than the other long-range corrected functionals, which is a direct consequence of tuning of the range separation parameter. When the oligomer length increases, the HOMO–LUMO gap energies of the optimized oligomers (see ESI, tables S5–S7) approach the HOCO–LUCO gap energies of the periodic models. However, the gap energies of the longest optimized oligomers are larger than the gap energies of the periodic models or those of the extrapolated gap values. In other words, the gap energy of the oligomers could still decrease, if the lengths of the oligomer chains were increased. This, in turn, means that the effect of conjugation, that reduces the band gap energy, exceeds eight (8) CRUs in the computational model of P1 and four (4) CRUs in those of P2 and P3. The extrapolated values are close to the values obtained by the PBC calculations, which suggests that both procedures are adequate for predicting the gap energy. However, a single PBC calculation is a more straightforward way to obtain the gap.

Because the calculated backbone dihedral angles vary according to the computational method, the effect of the chosen method on the HOMO–LUMO gap energy is not to be directly deduced from the gap energies presented in Table 4. The HOMO–LUMO gap energies are known to change as a function of the cosine of the dihedral angle x, see equation 3,[14,73] where E_{g0} is the HOMO–LUMO gap when dihedral angle in the model is 0 degrees and E_{g90} is the HOMO–LUMO gap when the dihedral angle in the model is 90 degrees. In order to study the effect of the variation of the dihedral angle on the gap, we compared the gaps of the partially optimized periodic model of P1, *i.e.* the dihedral angle α_{P1} (see Figure 1) was frozen to (0–90) degrees with increments of 10 degrees. The calculated HOCO–LUCO gaps are listed in Table 5. The models of P2 or P3 were not inspected, because they contain multiple different dihedral angles in the backbones of the CRUs. Additionally, while the inspection would have been interesting for the OT-ωB97X functional, it requires optimizing of the range-separation parameter (ω) for each periodic model using oligomer models with predefined dihedral angles so the functional was left out.

$$E_g(x) = E_{g0} + \left(E_{g90} - E_{g0}\right) * (1 - \cos x). \quad (3)$$

Formatted:

Table 5. HOCO–LUCO gaps (eV) of the partially optimized periodic model of P1 calculated with the predefined dihedral angles (°).

Method	0°	10°	20°	30°	40°	50°	60°	70°	80°	90°	E_{g90}-E_{g0}
PBE	**1.00**[a]	1.02	1.07	1.15	1.25	1.37	1.50	1.64	1.77	1.87	0.87
M06L	**1.13**	1.15	1.21	1.29	1.39	1.51	1.66	1.80	1.95	2.10	0.97
HSE06	**1.62**	1.65	1.73	1.84	1.98	2.14	2.31	2.49	2.66	2.78	1.16
B3LYP	**2.01**	2.04	2.13	2.25	2.39	2.55	2.73	2.91	3.07	3.17	1.17
PBE0	**2.28**	2.31	2.41	2.53	2.68	2.85	3.03	3.22	3.40	3.51	1.23
M06	**2.37**	2.41	2.49	2.61	2.75	2.90	3.07	3.25	3.41	3.56	1.19
M06-2X	3.85	**3.89**	4.00	4.14	4.30	4.49	4.69	4.90	5.11	5.26	1.41
ωB97XD	5.32	5.37	**5.49**	5.64	5.83	6.03	6.24	6.45	6.65	6.76	1.44
LC-ωPBE	6.27	6.32	**6.45**	6.62	6.81	7.01	7.23	7.45	7.65	7.76	1.50
M06-HF	6.46	6.52	**6.64**	6.81	7.00	7.21	7.44	7.67	7.87	7.99	1.54
HF	7.04	7.13	7.32	**7.53**	7.76	8.00	8.25	8.50	8.70	8.80	1.76

[a] Results closest to the fully optimized model of P1 (for angles see Table 2 and for gaps see Table 4) are in boldface.

The HOCO–LUCO gap energy increases when the dihedral angle increases. While the values do not exactly fit the equation 3 they still change roughly as a function of (1- cos *x*), meaning that the gap energy changes only little when the dihedral angle *x* is small, but larger changes result as soon as the dihedral angle is (30–60) degrees. Because the methods predict small dihedral angles in the backbone of the geometry of the optimized P1, the effect of the geometry on the gap energy is negligible with most of the methods and modest, i.e. up to 0.2 eV, with the high HF exchange DFT functionals (ω-functionals). In the case of the HF method the planar P1 has a gap of 7.04 eV (Table 5) and the optimized P1 that has a dihedral angle of 32° (Table 2) has a gap of 7.57 eV (Table 4) meaning that the gap has increased 7 % due to the change of the dihedral angle. In the case of polymers P2 and P3 the predicted dihedral angles are (12–37)° for α_{P2}, (2–17)° for β_{P2}, (16–37)° for α_{P3}, and (40–54)° for β_{P3} (Table 2). Because the angles vary this much the HOMO – LUMO gap difference arising from the dihedral angle difference can be expected to be bigger. The gap energies at different dihedral angles also demonstrate why the planarity of the polymer is desired when a narrow HOMO–LUMO gap is pursued.

Effect of the method on the first electronic excitation

Next we examined the TD-DFT and TD-HF gaps of the polymers. The energies of the first (vertical) excitations (S0 → S1) of the longest oligomers and the corresponding extrapolated excitation energies of the polymers are presented in Table 6. The first excitation energies are mainly from HOMO to LUMO and are presented as a function of the oligomer length in ESI.

Table 6. First TD-DFT and TD-HF excitation energies (eV) of the longest oligomers and the corresponding values (eV) extrapolated to the polymer limit. Experimental values[a] are from references ~~37~~37 (P2, P3) and ~~38~~38 (P1).

Method	P1		P2		P3	
	n=8	extrapolated	n=4	extrapolated	n=4	extrapolated
PBE	1.08	0.98	1.32	1.15	1.53	1.40
M06L	1.21	1.11	1.43	1.26	1.66	1.53
HSE06	1.68	1.57	1.95	1.85	2.24	2.14
B3LYP	1.80	1.72	2.03	1.96	2.31	2.24
PBE0	1.95	1.87	2.20	2.12	2.49	2.44
M06	1.94	1.86	2.16	2.10	2.42	2.33
M06-2X	2.61	2.58	2.79	2.71	3.11	3.04
OT-ωB97X	2.26	-	2.51	-	2.93	-
OT-ωB97X$_{solv}$	*	-	2.44	-	2.88	-
ωB97XD	2.82	2.78	2.93	2.89	3.30	3.27
LC-ωPBE	3.26	3.20	3.38	3.30	3.79	3.73
M06-HF	3.42	3.37	3.57	3.51	3.92	3.86
HF	3.59	3.53	3.62	3.53	4.10	4.06

Absorption maxima measured in chloroform solutions are 2.03 eV (P1), 2.32 eV (P2), and 2.80 eV (P3) and the optical band gaps estimated from the onset wavelengths of the UV-Vis spectra of thin films are 1.91 eV (P1), 2.08 eV (P2), and 2.34 eV (P3). *Too demanding to calculate.

Except in the case of the OT-ωB97X$_{solv}$ functional, the solvent effects have been neglected in the calculations. Moreover, the basis set is rather small. Therefore, the results are expected to deviate from the experimental quantities and a direct comparison between the calculated and experimental results cannot be done. However, when the same oligomer is studied using different density functionals, the 6-31G* basis set and the lack of the solvation model do not remarkably affect the relative results. The first excitation energy increases as the amount of the exact HF exchange in the method increases, as in the case of the HOMO–LUMO gaps (Table 4). The OT-ωB97X functional yields the smallest excitation energies of the high HF exchange methods and the results look very promising if compared to the experimental data. For this reason we performed additional calculations with the 6-31+G(d,p) basis set and chloroform as a solvent for a better comparability with the experimental values. The excitation energies obtained from these calculations are slightly smaller than those calculated with the smaller basis set in vacuum. The results are also rather close to the experimental values with ca. 0.1 eV differences. However, there are still error sources left and we expect the most notable errors to come from the oligomer length and the consideration of only one conformer.

The excitation energies obtained for the longest oligomers are still (0.04–0.17) eV larger than the extrapolated values. It is good to note that the difference between the excitation energy of the longest oligomer and the extrapolated value is smaller with the high HF methods, meaning that these methods converge faster. However, it is possible that the energies would decrease further if a longer oligomer model was used, which means that the effect of the conjugation exceeds eight (8) CRUs in P1 and four (4) CRUs in P2 and P3.

Effect of the method on the HOMO and LUMO and their electron densities

The electron density distributions on the frontier molecular orbitals (FMOs) were examined with the chosen methods. The HOMO is expected to be concentrated on the electron rich donor parts and the LUMO on the electron deficient acceptor parts of the polymer. Benzodithiophene is the electron rich part and 2-phenyl benzotriazole the electron deficient part in P1. In P2 and P3 fluorene and thiophene are rich in electrons and 2-phenyl benzotriazole is electron deficient. The contributions of the electron density distributed on the donor (D) and acceptor (A) units of the polymer backbone to HOMO, LUMO, HOCO, and LUCO are presented in Tables 7a–c.

Table 7a. Contributions (%) of the electron densities of the D[a] and A[b] units of the polymer backbone to FMOs in the models of P1.

Method	P1 oligomer				P1 periodic			
	HOMO		LUMO		HOCO		LUCO	
	D	A	D	A	D	A	D	A
PBE	76	24	40	60	76	24	40	60
M06L	75	25	39	61	75	25	39	61
HSE06	75	25	41	59	75	25	41	59
B3LYP	74	26	40	60	74	26	40	60
PBE0	75	25	41	59	74	26	42	58
M06	75	25	40	60	74	26	40	60
M062X	75	25	42	58	74	26	43	57
OT-ωB97X	75	25	38	62	75	25	39	61
ωB97XD	75	25	40	60	74	26	42	58
LC-ωPBE	77	23	42	58	76	24	42	58
M06-HF	77	23	43	57	76	24	43	57
HF	75	25	38	62	75	25	39	61
PM6	94	6	31	69	-	-	-	-

[a] D = benzodithiophene; [b]A = benzotriazole.

Table 7b. Contributions (%) of the electron densities of the D [a], D' [b], and A[c] units of the polymer backbone to FMOs in the models of P2.

Method	P2 oligomer						P2 periodic					
	HOMO			LUMO			HOCO			LUCO		
	D	D'	A	D	D'	A	D	D'	A	D	D'	A
PBE	30	47	23	16	29	55	31	47	22	17	30	53
M06L	31	47	23	15	29	55	31	47	22	16	30	54
HSE06	30	46	23	15	29	56	31	46	23	16	30	55
B3LYP	30	46	23	14	29	57	31	46	23	15	29	56
PBE0	30	46	23	15	29	56	31	46	23	16	30	55
M06	31	46	23	14	28	59	32	46	23	15	28	57
M062X	30	46	24	14	28	57	31	46	23	15	29	56
OT-ωB97X	30	46	24	13	26	61	31	46	23	13	27	59
ωB97XD	30	46	24	12	26	62	31	46	24	13	27	60
LC-ωPBE	31	44	24	12	27	61	31	45	24	13	27	60
M06-HF	31	45	24	13	26	61	31	45	24	14	26	60
HF	36	42	22	11	24	64	35	42	22	12	26	62
PM6	39	36	25	2	15	82	-	-	-	-	-	-

[a] D = fluorene, [b] D'= thiophene, [c]A = benzotriazole.

Table 7c. Contributions (%) of the electron densities of the D [a], D' [b], and A[c] units of the polymer backbone to FMOs in the models of P3.

Method	P3 oligomer						P3 periodic					
	HOMO			LUMO			HOCO			LUCO		
	D	D'	A	D	D'	A	D	D'	A	D	D'	A
PBE	33	47	19	12	22	66	34	47	19	13	23	65
M06L	33	47	20	12	22	66	34	47	20	13	23	65
HSE06	35	46	19	11	22	67	35	46	19	12	22	66
B3LYP	36	46	18	10	20	70	36	46	18	11	21	68
PBE0	36	46	19	11	22	67	36	46	18	12	22	66
M06	36	45	19	10	21	68	36	45	19	11	22	67
M062X	36	45	19	12	22	66	36	45	19	13	23	64
OT-ωB97X	38	45	17	9	18	73	37	45	18	10	19	72
ωB97XD	38	44	17	9	19	72	39	44	17	10	19	71
LC-ωPBE	40	43	17	10	19	71	40	43	17	11	20	69
M06-HF	39	43	18	11	20	69	43	39	18	12	21	67
HF	50	37	13	9	16	76	49	38	13	10	16	74
PM6	34	41	25	2	25	73	-	-	-	-	-	-

[a] D = fluorene, [b] D'= thiophene, [c]A = benzotriazole.

The computational method affects the distribution of the electron density only slightly (up to four percentage point difference) in the models of P1, excluding the PM6 method that yields a very strongly

localized HOMO and a bit more localized LUMO compared to the other methods. The models of P2 have up to nine percentage point variation in the electron density contributions when calculated with different methods, excluding PM6. The HF method yields more localized orbitals than the DFT methods. In the case of the P3 models up to 17 percentage point variation is seen in the results between the different DFT methods. Also the electron density of HOMO is more localized in donors and LUMO is more localized in acceptors in the models of P3 than in those of P2 by roughly five to ten percentage points. This is probably caused by larger backbone dihedral angles in P3, which hinder the delocalization along the chain. The optimally tuned OT-ωB97X functional yields results similar to the other high HF exchange methods when we compare the electron density distribution of the highest occupied orbital. However, there are differences when the electron density distributions of the first unoccupied orbitals are considered. In the case of the P1 models the electron density values differ from those calculated using the other high HF exchange methods and the electron density is localized largely on the acceptor. In the case of the P2 models the results are similar to those yielded by the other high HF exchange functionals. In the case of the P3 models, however, a larger amount of an electron density is again localized on the acceptor.

The polymer model affects the distribution of the electron density, as well. In the oligomer models the FMO electron density is the strongest in the middle of the model and almost non-existent at the terminating ends. In the periodic models, instead, the electron density is evenly distributed along the same CRUs as is evident from the molecular orbitals, see Figure 3. This is because the energy levels are equivalent in the periodic models but split in the oligomer models. However, the total distribution of the FMO electron density between the donors and acceptors is similar in both polymer model types, as is seen in Tables 7a–c. As such, it can be said that both the oligomer model and the PBC model can be used to analyze the electron density.

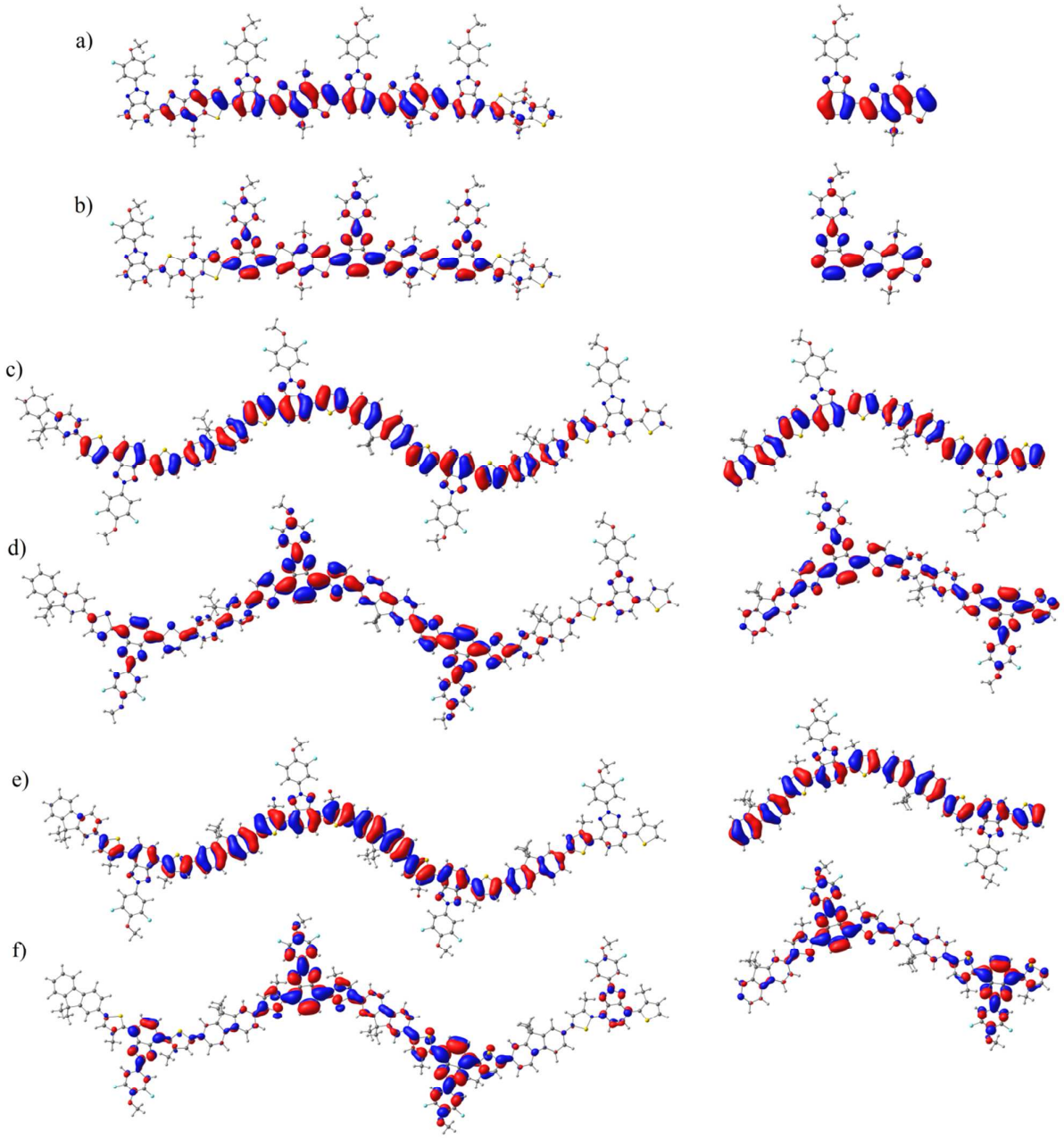

Figure 3. Frontier molecular (left)/crystal (right) orbitals of the oligomer models (left) and the PBC models (right): a) P1 HOMO b) P1 LUMO, c) P2 HOMO, d) P2 LUMO, e) P3 HOMO, f) P3 LUMO. The B3LYP/6-31G* level of theory was used. The electron density is obtained by squaring the wavefunction.

Conclusions

We have evaluated various computational methods and both oligomer and periodic models in predicting structural and electronic properties of three conjugated donor–acceptor polymers used in experimental photovoltaic cell devices. We used the HF wavefunction method, the PM6 semiempirical method, and DFT with 11 different functionals, *i.e.* B3LYP, PBE, PBE0, HSE06, LC-ωPBE, ωB97XD, OT-ωB97X, M06, M06L, M062X, and M06HF.

The polymers studied do not contain strong planarity enforcing interactions, and therefore, the method affects the dihedral angles of the polymer backbone. There is a clear correlation between the amount of the exact HF exchange in the method and the value of the dihedral angle in both the oligomer and periodic models. The increase in the amount of the HF exchange increases the dihedral angle by (20–30)° when going from the pure density functionals via the hybrid functionals and the functionals containing high amounts of the exact HF exchange to the pure HF method. It is notable, that the density functionals that do not contain exact HF exchange promote more planar structures. On the other hand, the pure functionals predict the smallest BLA values (less conjugated structures) and the values increase as the amount of the exact HF exchange increases in the method. This is because the pure DFT functional predict structures where the electrons are overly delocalized and when the amount of the exact HF exchange increases the electrons become more localized and the BLA value increases.

The results for the optimally tuned OT-ωB97X functional were of specific interest as the use of the optimally tuned functionals may lead to a much greater accuracy in conjugated polymers. The optimally tuned values for the range-separation parameter were down to (0.16–0.10) $bohr^{-1}$ from the initial value of 0.30 $bohr^{-1}$. This indicates that a higher degree of delocalization than in the normal long-range corrected functionals is necessary. The dihedral angles in the polymer backbones are of a similar size as obtained with the other high HF exchange functionals and the bond length alternation is smaller than with the typical high HF exchange functionals but larger than with the hybrid functionals. The predicted HOMO–LUMO and HOCO–LUCO gaps fall between the M062X and ωB97XD functionals and the energy of the first excitation calculated with TD-DFT is below the values obtained with M062X but above the values obtained with the hybrid functionals. The TD-DFT calculations with the 6-31+G(d,p) basis set and the solvent model yielded results within 0.1 eV of the experimental values highlighting the usefulness of the OT functionals.

The results are similar for both the oligomer and periodic models. With periodic models there is no need to extrapolate, making their use easier. However, when for example empirical dispersion correction or TD formalism is needed they are not readily available in all the codes that provide PBCs. In the case of the optimally tuned range-separated functional, the PBC approach is intriguing, but requires tuning of the range separation parameter either with long oligomers or possibly through the fitting of the results calculated for the shorter oligomers.

Acknowledgements

Financing of the computational research by the Academy of Finland is greatly appreciated. An incentive grant from Emil Aaltonen Foundation is gratefully acknowledged. Computing resources provided by the CSC – IT Center for Science Ltd, administrated by the Finnish Ministry of Education, are acknowledged. We thank Professor Gustavo Scuseria, Dr. Melissa Lucero, and M.Sc. Ireneusz Bulik at Rice University, Houston, Texas, for their hospitality and fruitful discussions. We are also grateful for prof. J.-L. Brédas and Dr. Chad

Risko at Georgia Institute of Technology, Atlanta, USA for the improving comments on this work and the discussions, e.g. on the extrapolation methods.

Notes and references

[a]Department of Chemistry and Bioengineering, Tampere University of Technology, Korkeakoulunkatu 8, P.O. Box 541, Tampere, FI-33101, FINLAND

Electronic Supplementary Information (ESI) available: Assessment of exact HF exchange, bond paths used in BLA and detailed information of obtained BLA, more detailed information of obtained HOMO – LUMO gaps and 1st excitation energies and the procedure used to extract the electron density contributions.

1 C. R. Towns, I. Grizzi, M. Roberts, A. Wehrum, *J. Lumin.*, 2006, **122–123**, 976–979.
2 J. Shin, H. A. Um, M. J. Cho, T. W. Lee, K. H. Kim, J.-I. Jin, S. Kang, T. Park, S. H. Joo, J. H. Yang, D. H. Choi, *J. Polym. Sci. Part A: Polym. Chem*, 2012, **50**, 388–399.
3 H.-W. Lin, W.-Y. Lee, W.-C. Chen, *J. Mater. Chem.*, 2012, **22**, 2120–2128.
4 L. Dou, J. You, J. Yang, C.-C. Chen, Y. He, S. Murase, T. Moriarty, K. Emery, G. Li, Y. Yang, *Nat. Photonics*, 2012, **6**, 180–185.
5 G. Li, R. Zhu, Y. Yang, *Nat. Photonics*, 2012, **6**, 153–161.
6 Y. Liu, Q. Miao, S. Zhang, X. Huang, L. Zheng, Y. Cheng, Macromol. Chem. Phys., 2008, **209**, 685–694.
7 X. Wu, B. Xu, H. Tong, L. Wang, *Macromolecules*, 2011, **44**, 4241–4248.
8 S. S. Pinnock, C. N. Malele, J. Che, W. E. Jones Jr., *J. Fluoresc*, 2012, **22**, 583–589.
9 E. E. Havinga, W. ten Hoeve, H. Wynberg *Polym. Bull.* 1992, **29**, 119–126.
10 G. L. Gibson, T. M. McCormick, D. S. Seferos *J. Am. Chem. Soc.*, 2012, **134**, 539–547.
11 C.-C. Chen, L. Dou, R. Zhu, C.-H. Chung, T.-B. Song, Y. B. Zheng, S. Hawks, G. Li, P. S. Weiss, Y. Yang, *ACS Nano*, 2012, **6**, 7185–7190.
12 S. Xiao, A. C. Stuart, S. Liu, H. Zhou, W. You, *Adv. Funct. Mater.*, 2010, **20**, 635–643.
13 S. Habuchi, H. Fujita, T. Michinobu, M. Vacha, *J. Phys. Chem. B*, 2011, **115**, 14404–14415.
14 C. Risko, M. D. McGehee, J.-L. Brédas, *Chem. Sci.*, 2011, **2**, 1200–1218.
15 Y. Wang, Q. Peng, Q. Hou, K. Zhao, Y. Liang, B. Li, *Theor. Chem. Acc.*, 2011, **129**, 257–270.
16 Z. El Malki, S. M. Bouzzine, L. Bejjit, M. Haddad, M. Hamidi, M. Bouachrine, *J. Appl. Polym. Sci.*, 2011, **122**, 3351–3360.
17 A. Abbotto, M. Seri, M. S. Dangate, F. De Angelis, N. Manfredi, E. Mosconi, M. Bolognesi, R. Ruffo, M. M. Salamone, M. Muccini, *J. Polym. Sci., Part A: Polym. Chem.*, 2012, **50**, 2829–2840.
18 Z. Lin, J. Bjorgaard, A. G. Yavuz, A. Iyer, M. E. Köse, *RSC Adv.*, 2012, **2**, 642–651.
19 J. Torras, J. Casanovas, C. Alemán, *J. Phys. Chem. A*, 2012, **116**, 7571-7583.
20 L. Ling, J. B. Lagowski, *J. Mol. Struct. THEOCHEM*, 2010, **944**, 146–155.
21 B. G. Janesko, *J. Chem. Phys.*, 2011, **134**, 184105: 1–8.
22 J. M. Granadino-Roldán, A. Garzón, G. García, M. Moral, A. Navarro, M. P. Fernández-Liencres, T. Peña-Ruiz, M. Fernández-Gómez, *J. Phys. Chem. C*, 2011, **115**, 5865–2873.
23 T. M. Pappenfus, J. A. Schmidt, R. E. Koehn, J. D. Alia, *Macromolecules*, 2011, **44**, 2354–2357.
24 A. Ferretti, G. Mallia, L. Martin-Samos, G. Bussi, A. Ruini, B. Montanari, N. M. Harrison, *Phys. Rev. B*, 2012, **85**, 235105: 1–15.
25 L. Deng, W. Shen, X. Xie, L. Jiang, B. Liu, M. Li, *Struct. Chem.*, 2012, **23**, 97–106.

26 S. Grimm, D. Tabatabai, A. Scherer, J. Michaelis, I. Frank, *J. Phys. Chem. B, 2007,* **111**, 12053-12058.
27 D. Beljonne, J. Cornil, L. Muccioli, C. Zannoni, J.-L. Brédas, F. Castet, *Chem.. Mater.*, 2011, **23**, 591–609.
28 Y.-T. Fu, C. Risko, J.-L. Brédas, *Adv. Mater.*, 2013, **25**, 878–882.
29 J. M. Frost, F. Cheynis, S. M. Tuladhar, J. Nelson, *Nano Lett.*, 2006, **6**, 1674–1681.
30 N. C. Miller, E. Cho, M. J. N. Junk, R. Gysel, C. Risko, D. Kim, S. Sweetnam, C. E. Miller, L. J. Richter, R. J. Kline, M. Heeney, I. McCulloch, A. Amassian, D. Acevedo-Feliz, C. Knox, M. R. Hansen, D. Dudenko, B. F. Chmelka, M. F. Toney, J.-L. Brédas, M. D. McGehee, *Adv. Mater.*, 2012, **24**, 6071–6079.
31 T. Van Regemorter, M. Guillaume, A. Fuchs, C. Lennartz, V. Geskin, D. Beljonne, J. Cornil, *J. Chem. Phys.*, 2012, **137**, 174708: 1–9.
32 T. Van Regemorter, M. Guillaume, G. Sini, J. S. Sears, V. Geskin, J.-L. Brédas, D. Beljonne, J. Cornil, *Theor. Chem. Acc.*, 2012, **131**, 1273: 1–8.
33 U. Salzner, A. Aydin, *J. Chem. Theor. Comput.*, 2011, **7**, 2568–2583.
34 J.-D. Chai, M. Head-Gordon, *J. Chem. Phys.*, 2008, *128*, 084106: 1–15.
35 L. Kronik, T. Stein, S. Refaely-Abramson, R. Baer, *J. Chem. Theor. Comput.*, 2012, *8*, 1515–1531.
36 D. Jacquemin, B. Moore, A. Planchat, C. Adamo, J. Autschbach, *J. Chem. Theor. Comput.*, 2014, *10*, 1677–1685.
37 F. M. Pasker, M. F. G. Klein, M. Sanyal, E. Barrena, U. Lemmer, A. Colsmann, S. Höger, *J. Polym. Sci., Part A: Polym. Chem.*, 2011, **49**, 5001–5011.
38 V. Manninen, M. Niskanen, T. I. Hukka, F. Pasker, S. Claus, S. Höger, J. Baek, T. Umeyama, H. Imahori, H. Lemmetyinen, *J. Mat Chem. A*, 2013, **1**, 7451-7462.
39 J. Kahovec, R. B. Fox, K. Hatada *Pure Appl. Chem.*, 2002, **74**, 1921-1956.
40 Gaussian 09, Revision B.01, M. J. Frisch, G. W. Trucks, H. B. Schlegel, G. E. Scuseria, M. A. Robb, J. R. Cheeseman, G. Scalmani, V. Barone, B. Mennucci, G. A. Petersson, H. Nakatsuji, M. Caricato, X. Li, H. P. Hratchian, A. F. Izmaylov, J. Bloino, G. Zheng, J. L. Sonnenberg, M. Hada, M. Ehara, K. Toyota, R. Fukuda, J. Hasegawa, M. Ishida, T. Nakajima, Y. Honda, O. Kitao, H. Nakai, T. Vreven, J. A. Montgomery, Jr., J. E. Peralta, F. Ogliaro, M. Bearpark, J. J. Heyd, E. Brothers, K. N. Kudin, V. N. Staroverov, T. Keith, R. Kobayashi, J. Normand, K. Raghavachari, A. Rendell, J. C. Burant, S. S. Iyengar, J. Tomasi, M. Cossi, N. Rega, J. M. Millam, M. Klene, J. E. Knox, J. B. Cross, V. Bakken, C. Adamo, J. Jaramillo, R. Gomperts, R. E. Stratmann, O. Yazyev, A. J. Austin, R. Cammi, C. Pomelli, J. W. Ochterski, R. L. Martin, K. Morokuma, V. G. Zakrzewski, G. A. Voth, P. Salvador, J. J. Dannenberg, S. Dapprich, A. D. Daniels, O. Farkas, J. B. Foresman, J. V. Ortiz, J. Cioslowski, and D. J. Fox, Gaussian, Inc., Wallingford CT, 2010.
41 J. J. P. Stewart, *J. Mol. Model.*, 2007, **13**, 1173–1213.
42 J. P. Perdew, K. Burke, M. Ernzerhof, *Phys. Rev. Lett.*, 1996, **77**, 3865–3868.
43 J. P. Perdew, K. Burke, M. Ernzerhof, *Phys. Rev. Lett.*, 1997, **78**, 1396.
44 Y. Zhao, D. G. Truhlar, *J. Chem. Phys.*, 2006, **125**, 194101: 1–18.
45 A. D. Becke, *J. Chem. Phys.* 1998, **98**, 5648–5652.
46 C. Lee, W. Yang, R. G. Parr, *Phys. Rev. B*, 1988, **37**, 785–789.
47 S. H. Vosko, L. Wilk, M. Nusair, *Can. J. Phys.* 1980, **58**, 1200–1211.
48 P. J. Stephens, F. J. Devlin, C. F. Chabalowski, M. J. Frisch, *J. Phys. Chem.* 1994, **98**, 11623–11627.
49 C. Adamo, V. Barone, *J. Chem. Phys.*, 1999, **110**, 6158–6169.
50 Y. Zhao, D. G. Thruhlar, *Theor. Chem. Acc.*, 2008, **120**, 215–241.
51 O. A. Vydrov, J. Heyd, A. V. Krukau, G. E. Scuseria, *J. Chem. Phys.*, 2006, **125**, 074106: 1–9.
52 O. A. Vydrov, G. E. Scuseria, *J. Chem. Phys.*, 2006, **125**, 234109: 1–9

53 Y. Zhao, D. G. Truhlar, *J. Phys. Chem.*, 2006, **110**, 5121–5129.
54 Y. Zhao, D. G. Truhlar, *J. Phys. Chem. A*, 2006, **110**, 13126–13130.
55 J.-D. Chai, M. Head-Gordon, *Phys. Chem. Chem. Phys.*, 2008, **10**, 6615–6620.
56 It is possible to use empirical dispersion correction with PBCs in Gaussian09 rev A.01, A.02, and B.01 even though it is not fully implemented. The empirical dispersion correction does not work across the cell boundaries and the periodic results presented here should be considered as estimates only.
57 T. Stein, L. Kronik, R. Baer, *J. Am. Chem. Soc.*, 2009, **131**, 2818–2820.
58 U. Salzner, R. Baer, *J. Chem. Phys*. 2009, **131**, 231101: 1–4.
59 J. Heyd, G. E. Scuseria, *J. Chem. Phys.*, 2004, **120**, 7274–7280.
60 J. Heyd, G. E. Scuseria, *J. Chem. Phys.*, 2004, **121**, 1187–1192.
61 J. Heyd, J. E. Peralta, G. E. Scuseria, R. L. Martin, *J. Chem. Phys.*, 2005, **123**, 174101: 1–8.
62 J. Heyd, G. E. Scuseria, M. Ernzerhof, *J. Chem. Phys.*, 2006, **124**, 219906: 1.
63 G. A. Zhurko, Chemcraft Version 1.60, available at www.chemcraftprog.com
64 M. Cossi, N. Rega, G. Scalmani, V. Barone, *J. Comput. Chem*., 2003, **24**, 669–681.
65 M. Niskanen, V. Manninen, T. I. Hukka, H. Lemmetyinen: Conjugated polymers in photovoltaic cells – a modeling study. International Conference on Science and Technology of Synthetic Metals, ICSM 2012, July 9–13, 2012. Atlanta, Georgia, USA. PI63
66 T. I. Hukka, M. Niskanen, V. Manninen, H. Lemmetyinen: Modeling of conjugated polymers tested in photovoltaic cells. Theory and Applications of Computational Chemistry, TACC-2012, September 2–7, 2012. University of Pavia, Pavia, Italy. p. 127.
67 C. B. Corman, S. R. Marder, *Proc. Natl. Acad. Sci. USA*, 1993, **90**, 11297–11301.
68 S. Suramitr, W. Meeto, P. Wolschann, S. Hannongbua, *Theor. Chem. Acc.*, 2010, **125**, 35–44.
69 W. Kuhn, *Helv. Chim. Acta*, 1948, **31**, 1780-1799.
70 G. Sini, J. S. Sears, J.-L. Brédas, *J. Chem. Theory Comput.*, 2011, **7**, 602–609.
71 N. E. Jackson, B. M. Savoie, K. L. Kohlstedt, M. O. de la Cruz, G. C. Schatz, L. X. Chen, M. A. Ratner, *J. Am. Chem. Soc.*, 2013, **135**, 10475–10483.
72 N. E. Jackson, B. M. Savoie, K. L. Kohlstedt, T. J. Marks, L. X. Chen, M. A. Ratner, *Macromolecules*, 2014, **47**, 987–992.
73 J. L. Brédas, G. B. Street, B. Thémans, J. M. André, *J. Chem. Phys.*, 1985, **83**, 1323–1329.